Acta Oceanologica Sinica 2008, Vol. 27, Supp., p. 129 ~ 144
http://www.oceanpress.com.cn
E-mail: hyxbe@263.net

Patterns of upper layer circulation variability in the South China Sea from satellite altimetry using the self-organizing map

LIU Yonggang[1*], WEISBERG Robert H[1], YUAN Yaochu[2]

1. College of Marine Science, University of South Florida, 830 First Street South, St. Petersburg, Florida 33701, USA
2. State Key Laboratory of Satellite Ocean Environment Dynamics, Second Institute of Oceanography, State Oceanic Administration, Hangzhou 310012, China

Received 4 February 2006; accepted 15 June 2006

Abstract

Patterns of the South China Sea (SCS) circulation variability are extracted from merged satellite altimetry data from October 1992 through August 2004 by using the self-organizing map (SOM). The annual cycle, seasonal and inter-annual variations of the SCS surface circulation are identified through the evolution of the characteristic circulation patterns. The annual cycle of the SCS general circulation patterns is described as a change between two opposite basin-scale SW-NE oriented gyres embedded with eddies: low sea surface height anomaly (SSHA) (cyclonic) in winter and high SSHA (anticyclonic) in summer half year. The transition starts from July—August (January—February) with a high (low) SSHA tongue east of Vietnam around 12° ~ 14° N, which develops into a big anticyclonic (cyclonic) gyre while moving eastward to the deep basin. During the transitions, a dipole structure, cyclonic (anticyclonic) in the north and anticyclonic (cyclonic) in the south, may be formed southeast off Vietnam with a strong zonal jet around 10° ~ 12° N. The seasonal variation is modulated by the interannual variations. Besides the strong 1997/1998 event in response to the peak Pacific El Niño in 1997, the overall SCS sea level is found to have a significant rise during 1999 ~ 2001, however, in summer 2004 the overall SCS sea level is lower and the basin-wide anticyclonic gyre becomes weaker than the other years.

Key words: circulation patterns, self-organizing map, satellite altimetry, annual cycle, inter-annual variation, South China Sea

1 Introduction

As the largest semienclosed marginal sea in the northwest Pacific, the South China Sea (SCS) has received its attention in oceanography research. One of the basic but important research efforts is to understand the patterns of ocean circulation variability. Early knowledge on the surface circulation patterns was inferred from ship drift data (Dale, 1956), or comprehensive hydrography, sea level and drifts (Wyrtki, 1961). Seasonal circulation patterns were later also derived from climatological hydrography

Foundation item: Yuan Yaochu was supported by National Basic Research Program of China under contract No. 2007CB816003, the Key International Cooperative Proiect of the National Natural Science Foundation of China under contract No. 40510073 and the International Cooperative Proiect of the Ministry of Science and Technology of China under contract No. 2006DFB21630.

* Corresponding author, E-mail: yliu18@gmail.com

(Zhou et al., 1995; Xu et al., 1982) and historical temperature profiles (Qu, 2000). Early in situ observations were limited to local areas, such as the northern SCS (e.g., Qiu et al., 1985), the central SCS (e.g., Chou, 1982) and the southern SCS (e.g., Fang, Guo et al., 1998). In 1998, hydrographic surveys covering the whole SCS were started, and basin-wide ocean currents were estimated and compared with the ship-board acoustic Doppler current profiler (ADCP) data (e.g., Yuan et al., 2005; Yuan et al., 2004; Xu et al., 2001; Liu et al., 2000); however, the number of the cruises covering the whole SCS was quite limited. It is hard to get spatial and temporal variability of the SCS circulation from in situ observations. Numerical models were also pursued to obtain the circulation patterns in the SCS (e.g., Wang et al., 2004; Cai et al., 2002; Metzger and Hurlburt, 2001; Takano et al., 1998; Shaw and Chao, 1994; Li et al., 1992; Liu and Su, 1992; Zeng et al., 1989; Pohlmann, 1987). For any numerical model, however, the real ocean dynamics is simplified in one way or another, also reliable circulation patterns output from a numerical ocean model are heavily relied on accurate initial and boundary conditions.

Satellite remote sensing opened a new era in ocean observations with the possibility of observing ocean circulation patterns continuously and in relatively large spatial coverage. Especially, satellite altimetry data can provide valuable information for ocean circulation (e.g., Jacobs et al., 2001; Fu and Cheney, 1995). Since 1995, satellite altimetry has been used to derive the SCS surface circulation patterns for many times (e.g., Wang et al., 2000; Liu and Xie, 1999; Mao et al., 1999; Shaw et al., 1999; Soong et al., 1995). Depending on the availability, different researchers used different data versions (duration and available satellites) as well as different technologies in extracting the characteristic patterns. Generally, two methods are used: temporal averaging and empirical orthogonal functions (EOF) analyses. Temporal averaging may be the simplest method, which has been applied to satellite altimetry for SCS circulation patterns, such as monthly mean patterns (Li et al., 2003; Liu et al., 2001; Ho, Zheng et al., 2000; Hwang and Chen, 2000) and seasonal average maps (Bao et al., 2005; Liu et al., 2001; Li et al., 2000; Morimoto et al., 2000). While averaging is useful, it is generally difficult to define suitable time scales over which to average, especially for the SCS where circulation and eddy patterns are very complex and currents may be anisotropic and nonhomogeneous depending on the processes and time scales involved (e.g., Guan and Yuan, 2006; Wu et al., 2005; Wang et al., 2003; Li, 2002; Hu et al., 2000; Su et al., 1999; Fang et al., 1998). EOF analyses are effective for reducing large correlated data sets into a smaller number of patterns ordered by variance, and applications to SCS altimetry data are given, for example, by Shaw et al. (1999), Ho, Kuo et al. (2000), and Chu et al. (2003). However, as a linear method conventional EOF is of limited use in extracting nonlinear information (Hsieh, 2001).

The self-organizing map (SOM), based on unsupervised neural network (Kohonen, 2001, 1982), is an effective method for feature extraction and classification. SOM applications have been found amongst various disciplines (e.g., Oja et al., 2002; Kaski et al., 1998), including climate and meteorology (e.g., Hong et al., 2005; Hsu et al., 2002; Cavazos, 2000). Recently, SOM analyses have also been applied to sea surface temperature (SST) and wind pattern extractions from satellite data (Richardson et al., 2003; Risien et al., 2004; Liu, Weisberg and He, 2006) and ocean current pattern extractions from moored ADCP data (Liu and Weisberg, 2007, 2005) and high frequency radar data (Liu et al., 2007). Some advantages identified for the SOM, relative to the EOF, are that data gaps are accommoda-

ted, temporal mean fields are retained and, more importantly, asymmetric patterns not found in individual EOF modes are extracted by the SOM (Liu and Weisberg, 2007, 2005; Liu, Weisberg and He, 2006; Liu, Weisberg and Mooers, 2006). These previous applications suggest that the SOM may be a more natural way to extract the SCS ocean circulation patterns from satellite altimetry data.

The present paper applies the SOM in analysis of multiyear satellite altimetry data. The purposes are two-fold. The first is to examine characteristic spatial and temporal patterns of ocean circulation and eddies in the SCS. The second is to demonstrate the usefulness of the SOM technology in analyzing satellite altimetry data. The rest of this paper is arranged as follows: After a brief description of the data set, small (2 × 2) and larger (3 × 4) size SOMs are applied to the SCS satellite altimetry data to extract the general features and more detailed patterns of SCS circulation, respectively; the characteristic patterns revealed by the SOM are then compared with and verified by the monthly mean climatology; analyses focus on seasonal and interannual time scales; attention is paid to new insights of the SOM results; in the end, a summary and discussions are provided.

2 Data

SSH anomaly (SSHA) data were downloaded from AVISO (archiving, validation and interpretation of satellite oceanographic data) website (http://las.aviso.oceanobs.com/las/servlets/dataset). The sea-level anomalies are defined as differences between the observed SSH and the first seven-year mean sea level. These [(1/3)° × (1/3)°] gridded data were merged from all available altimeter missions (Topex/Poseidon, Jason-1, ERS-1/2, and ENVISAT) and sampled at 7d interval from October 1992 through August 2004. The merged data were chosen for this study because combining data from several satellites gives a better space/time resolution, and thus significantly improves the estimation of mesoscale circulation (Le Traon et al 2002; Le Traon et al., 2001; Ducet et al., 2000; Le Traon and Dibarboure, 1999). This product was processed with improved altimeter corrections and processing algorithms for instrumental errors, environment perturbations (wet tropospheric, dry tropospheric and ionospheric effects), ocean wave influence (sea state bias), the tide influence (ocean tide, earth tide and pole tide) and inverse barometer effect (SSALTO/DUACS User Handbook, 2004). Even though tidal corrections were performed in generating the SSHA data, only the data over the deep ocean area (water depth greater than 100 m) is used in this analysis. The SCS bathymetry is shown in Fig. 1.

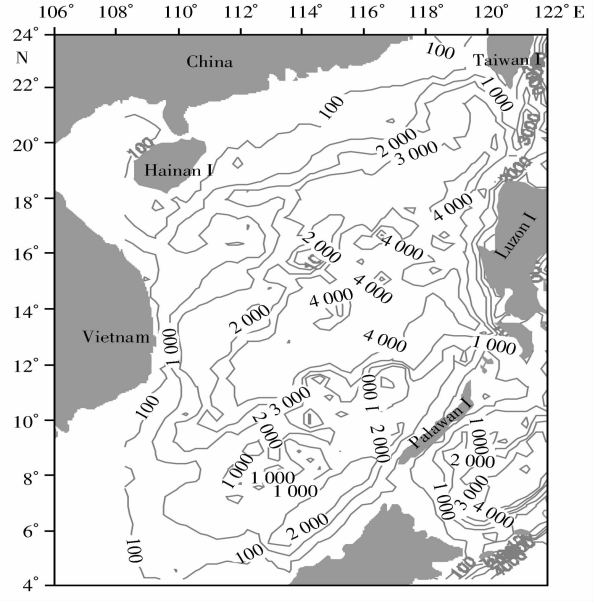

Fig. 1. Map of the South China Sea showing topography (isobaths unit in metre).

3 SOM performance

Prior to the neural network training process, tunable SOM parameters need to be specified. A practical method for choosing among the SOM parameters was given by Liu, Weisberg and Mooers

(2006). The first parameter is the map size, which defines how many neurons are used. A larger map size results in more detailed patterns, whereas a smaller map size results in more general patterns (Vesanto et al., 2000; Liu, Weisberg and Mooers, 2006). Thus, a small map size of 2 × 2 is first used to extract the SCS general ocean circulation patterns, and a larger map size of 3 × 4 is used to reveal more detailed patterns. The average quantization error (QE) monitors the quality of the SOM mapping during the training process. As the average distance between each data vector and the SOM best-matching unit (BMU), minimum QE indicates the most accurate representation of the input data. Given a rectangular lattice, "sheet" map shape, linearly initialized weights, and batch training as determined to be most appropriate in Liu, Weisberg and Mooers (2006), SOM analyses were repeated for different neighborhood functions and radii, and the resulting average QE was examined to search for the most accurate SOM mapping for the given map size. As expected from previous experiments, the "ep" neighborhood function with the radius of 1 provides the best choice (not shown).

4 General circulation patterns of annual cycle

4.1 Annual cycle from 2 × 2 SOM results

The small size 2 × 2 SOM is used to extract the general patterns of the SCS circulation variability from the 13a altimetry data. The four coherent SSHA patterns (and the associated anomalous geostrophic velocity fields) and the BMU time series are shown in Fig. 2. Pattern 1 shows a basin scale SW—NE oriented high SSHA (anticyclonic gyre) across the whole SCS with the center east off Vietnam (12° ~ 15°N) and to the south of the Xisha Islands. On both sides of this anticyclonic system, low SSHAs dominate the northern and southern SCS. Pattern 2 shows two high SSHAs in the northeastern and southwestern parts of the SCS. The NE high is stronger dominating the major northern SCS with the center northwest off Luzon (16° ~ 20°N), whereas the SE high is weaker controlling the southern SCS with the center southeast off Vietnam (8° ~ 11°N). Between these two highs, there is a low SSHA east of Vietnam and along the northwest SCS coast. Pattern 3 approximately mirrors Pattern 2, with two low SSHAs in the northeastern and southwestern parts of the SCS, respectively, and a high SSHA along the northwest SCS coast and east of Vietnam. More or less, Pattern 4 also mirrors Pattern 1. There is a basin scale SW—NE oriented low SSHA (cyclonic gyre) across the whole SCS embedded with three separate cyclonic eddies west off Luzon (17°N, 117°E), southeast off the Xisha Islands (15°N, 114 °E) and Vietnam (10°N, 111°E), respectively. On both sides of this low SSHA system, high SSHAs dominate the northwestern and southeastern SCS. There is a common feature for all the four patterns, i.e., the anomalous geostrophic currents on the western side of the SCS are stronger than those on the eastern side. Comparing the mirror patterns, the strongest anomalous geostrophic currents in SOM units 2 and 4 are stronger than those in SOM units 3 and 1, respectively.

The BMU time series show the evolution of these four patterns during the 12 years, in which a main feature of annual cycle is seen (Fig. 2, bottom panel). Generally, the sequence of the pattern evolution is 1→2→4→3→1. In summer half year the SCS circulation patterns are dominated by SOM units 1 (April—June) and 2 (July—September), and in winter half year they are dominated by SOM units 4 (October—December) and 3 (January—March) instead, as shown from Fig. 3.

4.2 Annual cycle from monthly mean climatology

Climatological monthly mean SSHA maps and the associated anomalous geostrophic velocities are

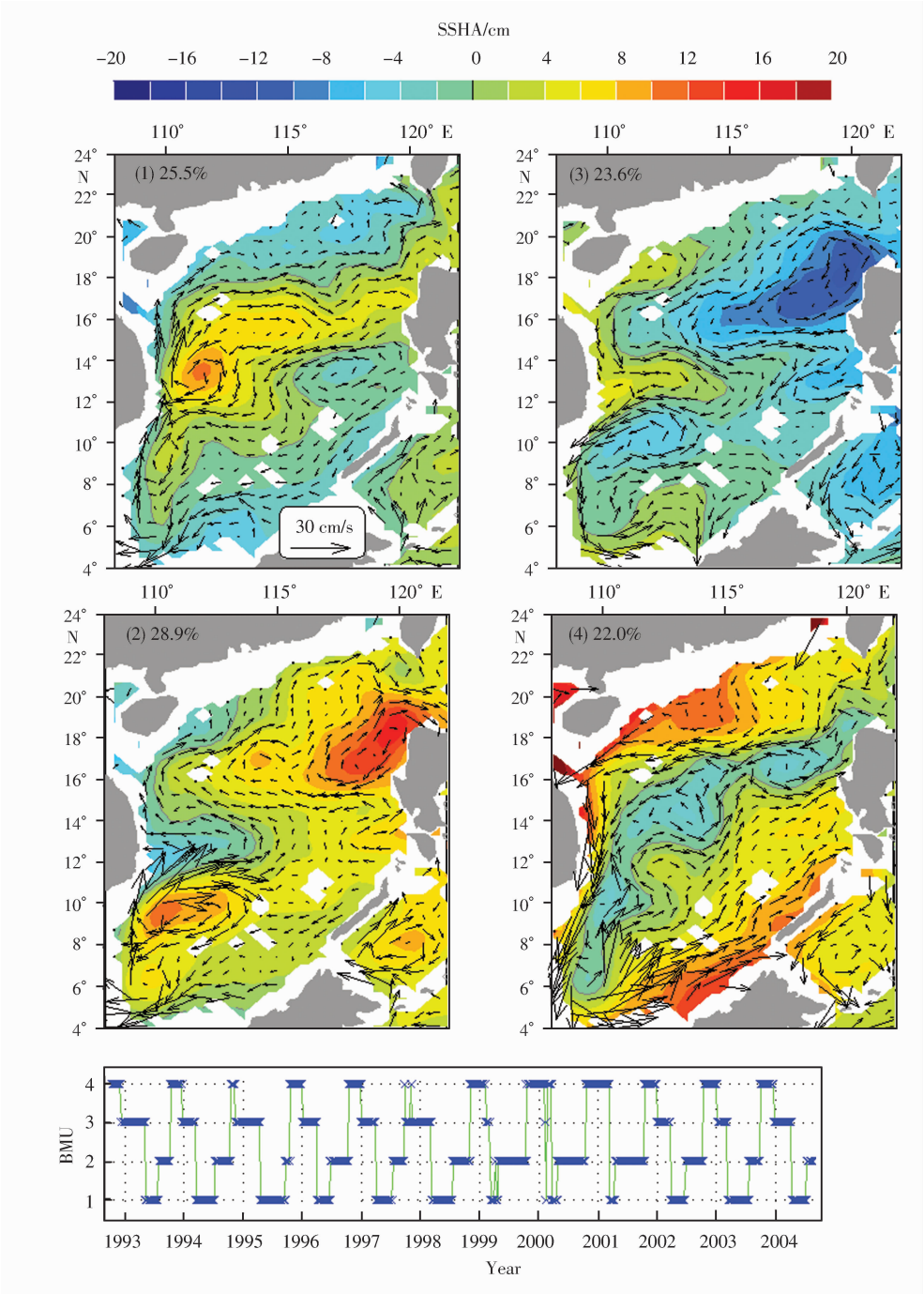

Fig. 2. A 2 × 2 SOM representation of the SSHA time series from October 1992 through September 2004. Upper four panels are the characteristic patterns of the SSHA overlain with their associated anomalous geostrophic currents. The frequency of occurrence is shown in the upper-left corner of each panel. Bottom panel shows time series of the best-matching unit for the above four patterns, with the ticks on the horizontal axis corresponding to January 1 of each year.

computed from the 13a weekly satellite altimetry data. The results are used to verify the SCS general circulation patterns of the annual cycle as revealed by the SOM, and to further examine the seasonal variation of the SCS surface circulation. From January through March, the whole SCS is dominated by low SSHA with two centers in the northeastern and southwestern parts of the SCS, respectively, and a

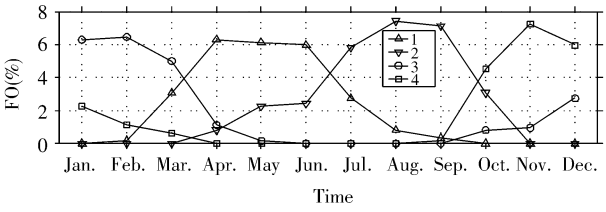

Fig. 3. Monthly frequency of occurrence (FO) of the individual SOM patterns in Fig. 2.

high SSHA along the northwest SCS coast and east of Vietnam. These features are in good agreement with those in the SOM unit 3 (Fig. 2) and its monthly frequency of occurrence (Fig. 3). From April to June, the general SSHA patterns (a basin scale SW—NE oriented high SSHA across the whole SCS) are in good agreement with those in the SOM unit 1. From July to September, the general SSHA patterns (two highs in the northeastern and southwestern parts of the SCS separated by relatively low SSHA east off Vietnam) are in good agreement with the SOM unit 2. The October pattern is a transition between the SOM units 2 and 4. Both the November and December patterns are pretty close to the SOM unit 4. In a word, the general circulation patterns of annual cycle extracted by the 2 × 2 SOM are confirmed by the monthly mean climatology.

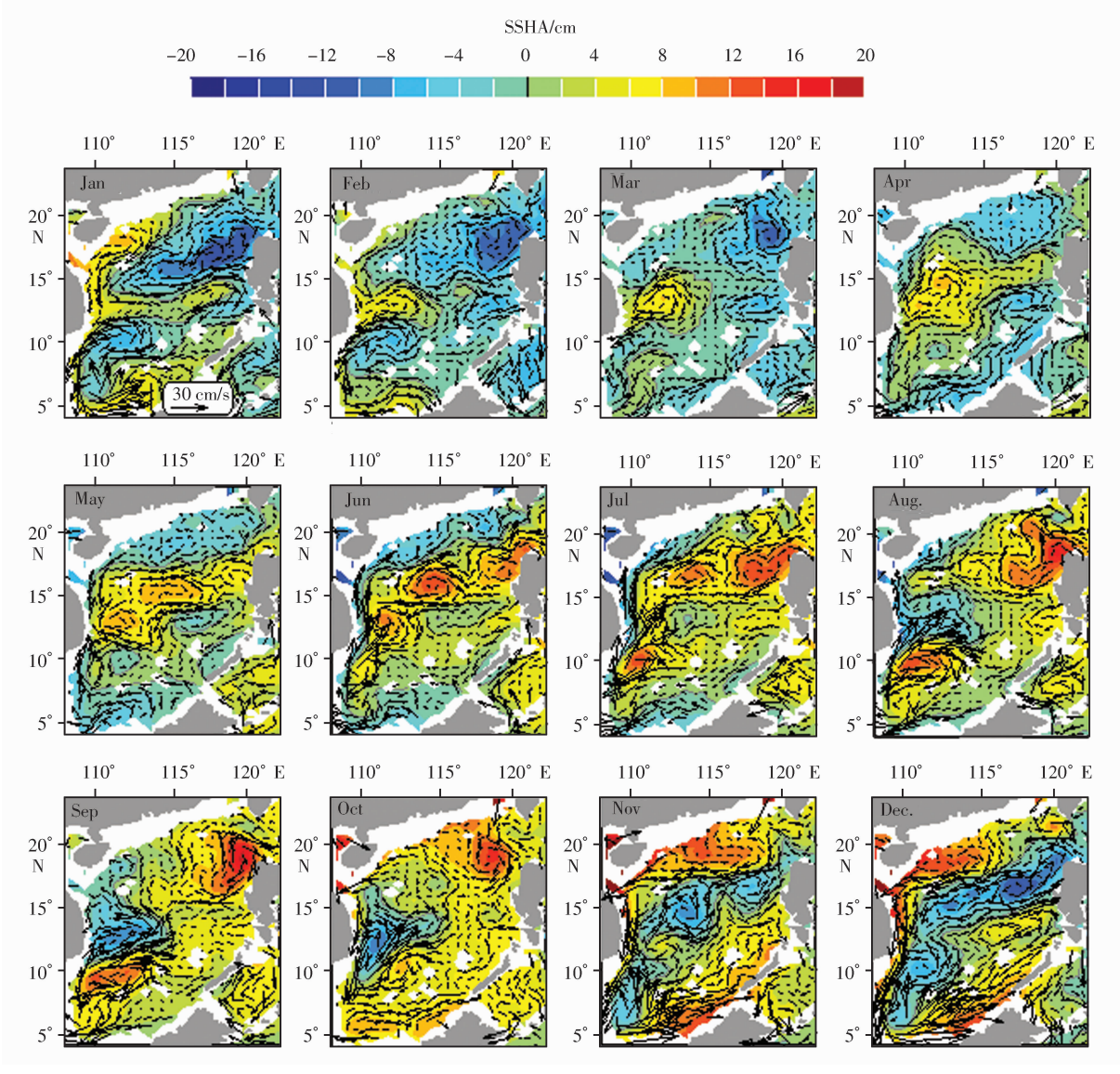

Fig. 4. Climatological monthly mean SSHA patterns and the associated anomalous geostrophic currents.

5 Seasonal variability

5.1 Seasonal variability from monthly mean climatology

Climatological monthly SSHA maps were also derived from the TOPEX/Poseidon data during 1993 ~ 1999 (Li et al., 2003; Hwang and Chen, 2000), and from the MSSHA (maps of sea surface height anomaly) products during 1992 ~ 2000 (Liu, Jia et al., 2001). It is useful to compare the new monthly patterns with the previous results to see whether new features are added in the new version of satellite altimetry product. Similar to those found by Hwang and Chen (2000), and Li et al. (2003), the SCS basin-wide circulation is generally cyclonic in winter months (November through February) and anticyclonic in summer months (May through July). There are two prominent features in the monthly SSHA fluctuations (and in the SOM results as well). One is the strong, basin-scale SW—NE directed SSHA across the SCS, low in winter and high in summer, which was reported by Li et al. (2003). The other is gradual growth of high (low) SSHA along 13°N east off Vietnam from February to April (from August to October), as pointed out by Li et al. (2003) and Hwang and Chen (2000). The strong anomalous geostrophic currents are found at the western boundary of the SCS, southward in winter and northward in summer, with the strongest currents east off the Vietnam coast; this is also in good agreement with the previous results (Hwang and Chen, 2000). Also, the seasonal variation of circulation in the southern SCS is more remarkable than that in the north, which is consistent with the previous findings of Liu, Yang et al. (2001).

New features are found from this version of monthly climatology. For example, zonal high SSHA ridge along 13°N east off Vietnam starts to appear from January, and it becomes stronger in February, but they are not obvious at all in these two months from Li et al. (2003) monthly mean SSHA maps. In March it turns into an anticyclonic eddy, and in April it becomes a basin-scale anticyclonic system, which is stronger than that of Li et al. (2003). The new monthly climatology provides a better description of the continuous growth of this high SSHA system. Also, the low SSHA east off central Vietnam in October is much larger than that in Li et al. (2003). Another improvement is the resolution of the mesoscale eddies in the SW—NE oriented anticyclonic system across the whole SCS in May, June and July; these eddies are not fully discerned in the previous monthly mean maps (Li et al., 2003; Liu, Jia et al., 2001; Hwang and Chen, 2000). These new features benefit from a better data set with higher spatial resolution and longer duration. It was the TOPEX/Poseidon data alone that were used by both Li et al. (2003) and Hwang and Chen (2000), which had lower spatial resolution.

5.2 Seasonal variability from 3 × 4 SOM results

The SCS circulation patterns were found to be complex and have multi-eddy structure from in situ observations of individual cruises (Xu et al., 2001; Liu et al., 2000; Su et al., 1999 ; Fang, Guo et al., 1998). The four patterns from the 2 × 2 SOM definitely cannot capture all the complex structures, as shown above in the monthly mean climatology. It is necessary to further examine the altimetry data with a larger size SOM for more detailed patterns of the SCS circulation variability. The SOM is applied to the altimetry data again with all the same tunable parameters except the map size, which is now set to be 3 × 4. The total number of the SOM patterns, i.e., 12, is the same as that from monthly mean climatology; thus the SOM results can be compared with the monthly mean maps to see whether the SOM provides new insights into the altimetry data.

The 3 × 4 SOM representation of the SCS circulation variability from the 13a weekly altimetry data is shown in Fig. 5. The spatial patterns are arranged on the SOM in such a way that similar patterns are located close to each other, and dissimilar patterns are located farther away from each other, with transitional patterns in between. Generally, lower SSHA patterns are located on the top row, whereas higher SSHA patterns are arranged to be in the bottom row of the SOM. Also, basin-wide cyclonic circulation patterns are located in the upper-right corner, whereas anticyclonic circulation patterns are located in the lower-left corner of the SOM; what between these two extremes are transitional patterns (Fig. 5, upper 12 panels). The temporal evolution of these spatial patterns is expressed in the BMU time series (Fig. 5, bottom panel), which shows that the SCS circulation has both seasonal and interannual variations.

Seasonal variation can be further studied by examining monthly frequency of occurrence of the individual SOM patterns. As shown in Fig. 6, Pattern 1 occurs from March through May with peak frequency of occurrence in April. Both Patterns 2 and 3 mainly occur from May through July, with peak frequency of occurrence in June. Pattern 4 mainly appears from January to April, and Pattern 5 from February to June. Both Patterns 6 and 8 appear mostly during July—October. Patterns 7 and 9 occur mostly during January—March and September—October, respectively. Patterns 10, 11 and 12 occur mostly from November through January, with peak frequencies of occurrence in January, December and November, respectively. These 12 patterns can be approximately divided into four categories: winter (Patterns 7, 10 ~ 12), spring (Patterns 1, 4 and 5), summer (Patterns 2 and 3), and fall (Patterns 6, 8 and 9). The winter patterns share a common characteristic: a basin-scale SW—NE oriented low SSHA associated with general cyclonic circulation within the SCS. In contrast, the summer patterns have a basin-scale SW—NE oriented high SSHA and anticyclonic general circulation. In the spring patterns, a high SSHA develops east off the central Vietnam around 13 N, a low SSHA is located northwest off the Luzon, and the currents are weak all over the SCS. In the fall patterns, there is a pair of eddies (the so-called "dipole") associated with an offshore jet east off the Vietnam coast and a high SSHA northwest off Luzon. As shown in the monthly mean frequencies of occurrence of these four categories, the seasonality of the SCS circulation may be defined as: winter (November—February), spring (March and April), summer (May—July), and fall (August—October) (Fig. 6e). This definition of the four seasons of the SCS circulation variability is the same as that by Li et al. (2003).

6 Interannual variability

Beyond the seasonal time scale, the SCS circulation exhibits interannual variation. As shown by the BMU time series (Fig. 5, bottom panel), the seasonal variation is modulated by the interannual variation. Before 1998 the winter circulation is dominated by Patterns 10 and 11, whereas after 1999 it is dominated by Pattern 12; the overall winter SSHA has a higher value and the general circulation associated with the basin-wide cyclonic gyre was weaker after 1999. The spring—summer circulation is dominated by Patterns 4, 1 and 2 before 1998, but by Patterns 5 and 3 during 1999 ~ 2001; the fall circulation is dominated by Pattern 8 before 1997 and after 2002, but by Patterns 6 and 9 during 1999 ~ 2001; both indicate an overall sea-level rise in the SCS during 1999 ~ 2001. Evidence of such interannual variation of the SSHA can be seen from the time series of spatial mean SSHA over the SCS with water depth greater than 100 m (Fig. 7). Previous reports on this interannual sea-level rise have not been found.

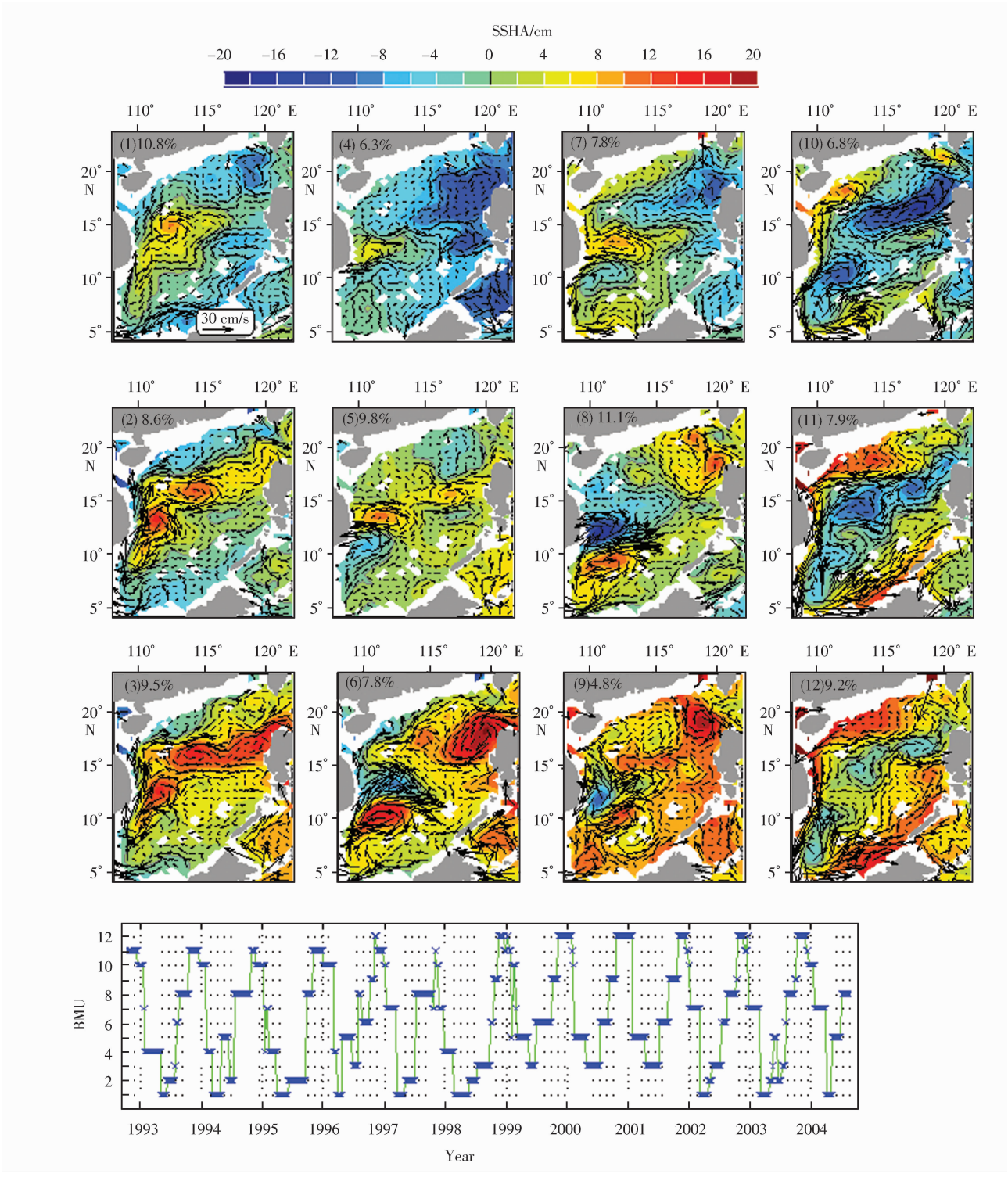

Fig. 5. Same as Fig. 2 but for a 3 × 4 SOM.

Noteworthy is the circulation in winter of 1997/1998. The occurrence of the typical winter Patterns 10, 11 and 12 is much lower than that of the other years (Fig. 5, bottom panel). The SCS circulation is reported to have an interannual variation related to El Niño/Southern Oscillation (e. g., Qu et al.,

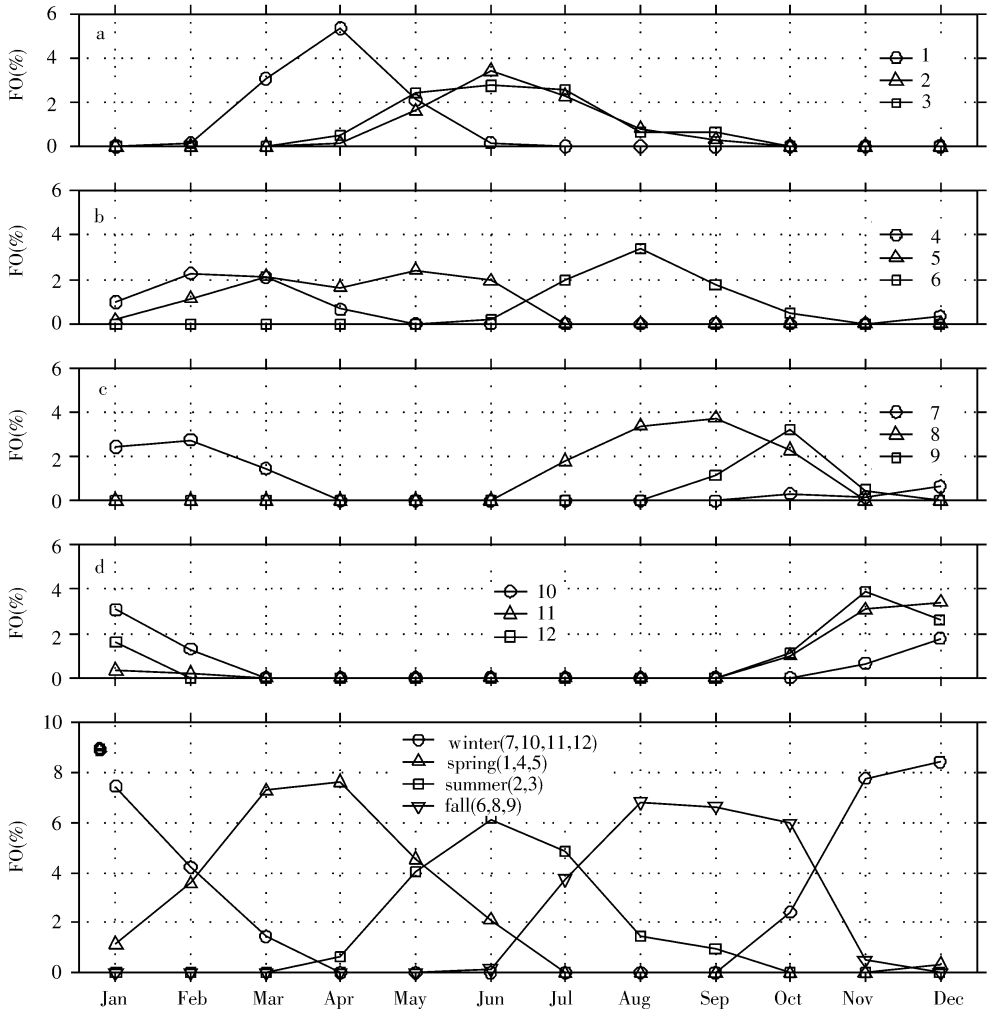

Fig. 6. Monthly frequency of occurrence (FO) of the individual SOM patterns in Fig. 5. a. Patterns 1 ~ 3, b. Patterns 4 ~ 6, c. Patterns 7 ~ 9, and d. Patterns 10 ~ 12. Bottom panel (e) shows the monthly FO of the four categories of the SOM patterns: winter (Patterns 7, 10 ~ 12), spring (Patterns 1, 4 and 5), summer (Patterns 2 and 3), and fall (Patterns 6, 8 and 9).

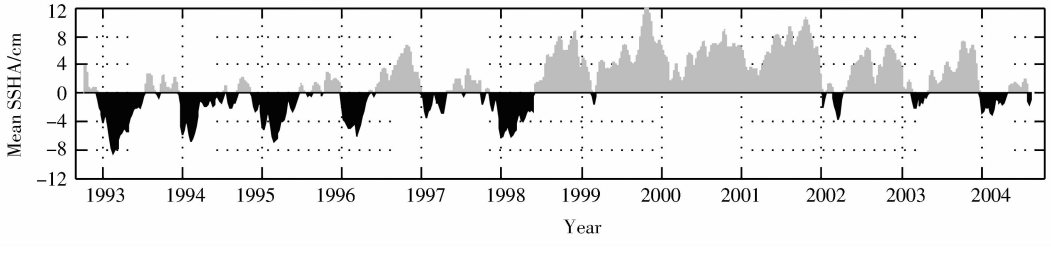

Fig. 7. Time series of spatial mean SSHA over the SCS with water depth greater than 100 m.

2005; Wu and Chang, 2005; Hwang and Chen, 2000; Ho, et al., 2000; Shaw et al., 1999; Wang et al., 1999; Wu et al., 1998). As shown in Wu and Chang (2005), Niño 3.4 index peaks in November 1997. The onset of 1997/1998 El Niño significantly weakens the prevailing northeasterly mon-

soon in December 1997, and then results in weaker circulation in winter of 1997/1998; thus it is Pattern 7, rather than Patterns 10 ~ 12, have higher occurrence in that winter.

Another interesting feature in 1998 is that Patterns 6 and 8, which often appear during July—October, are missing in August—September; instead, it is Pattern 3 that is seen (Fig. 5, bottom panel). That is to say, the dipole with an offshore monsoon jet southeast off Vietnam does not appear at all in August—September 1998. More specifically, both the low SSHA (cyclonic eddy) east off Vietnam usually around 12° ~ 13°N and the offshore jet are missing in those two months of 1998. This result is consistent with the previous findings of Xie et al. (2003) and Wu and Chang (2005) that the formation of the eastward jet and upwelling east off Vietnam is missing in July-August 1998, which is believed to be influenced by the Pacific ENSO in the previous year. As reported by Wang et al. (2002), there is a strong warm event during the entire year of 1998. The great summer warming of 1998 is explained as a result of both diminished wind jet east of Saigon, Vietnam, and suppressed mid-summer cooling (Xie et al., 2003).

Interannual modulation of the seasonal variation is also seen in summer 2004. As shown in Fig. 5 bottom panel, the circulation is dominated by Pattern 5 rather than by Patterns 2 and 3 (typical summer patterns). There is a low SSHA (cyclonic eddy) southeast off Vietnam, and the overall SSHA is lower than that in the other years; the latter is also seen in spatial mean SSHA (Fig. 7). Since it is seen in the recent data, no previous publication has been found on this phenomenon.

7 New insights from the SOM method

The usefulness of the SOM method in feature extraction has been demonstrated in many several recent physical oceanography applications (e.g., Liu amd Weisberg, 2007, 2005; Liu et al., 2007, 2006a, b). As a first-time application to the altimetry in the SCS, advantages of the SOM method can be seen by comparing the circulation patterns extracted by the SOM with those derived from other conventional methods, such as temporal averaging and EOF.

It is instructive to compare the 12 characteristic circulation patterns extracted by the 3 × 4 SOM with those from the monthly mean climatology. The SOM patterns are not simple averages of the data, they are derived from a nonlinear iterative learning process (neural network self-organizing); thus they summarize the data more accurately than the monthly mean maps. As shown in Figs 5 and 6, in the SOM results, one pattern may appear in several months, on the other hand, several patterns may be seen in one month. The 12 patterns may have different frequencies of occurrence. Temporal evolution of these patterns is also shown in the BMU time series. New insights into the patterns of the SCS surface circulation variability are obtained. For example, the dipole structure east off Vietnam, as seen in Patterns 6 and 8, can appear as early in July (Figs 6b and c), however, this structure is seen only in August and September in both the present climatological maps (see Fig. 4) and the previous studies (e.g., Hwang and Chen, 2000; Li et al., 2003). Also, the absolute low/high SSHA values in the center of the cyclonic/anticyclonic eddy west off Luzon (and many other eddies as well) are larger than those from the monthly mean maps. Thus, the strong currents (e.g., the monsoon jet) have larger velocities in the SOM patterns than in the climatological maps.

A comparison of the SCS ocean circulation patterns (SSHA) extracted by the SOM with those previously identified by the EOF also shows that new insights from the SOM are not readily seen in the EOF leading modes. For example, the dipole structure east off Vietnam coast is not shown in the

first two EOF modes (e.g., Shaw et al., 1999; Ho et al., 2000). Although this pattern is shown in the fourth EOF mode by Chu et al. (2003), the variance accounted for by this mode is less than 7%, and its statistical significance is not known. What is more, the evolution of the characteristic spatial patterns is shown in the BMU time series. One can easily identify the sequence of the pattern evolution in the SOM results, but that is not readily identifiable from the EOF results. From this point of view, the SOM patterns are more intuitive than the EOF patterns.

8 Summary and discussion

The SOM is used to extract the characteristic patterns of the SCS ocean circulation variability from the merged satellite SSHA data during the 13a from October 1992 to August 2004. Annual cycle, seasonal and interannual variations of the SCS circulation patterns are described based on the SOM results and climatological mean patterns.

The 2 × 2 SOM provides highly abstracted circulation patterns of annual cycle, which is better explained together with the monthly mean climatology of the SSHA. The annual cycle of the SCS general circulation patterns is synthesized as a gradual change between two opposite basin-scale SW—NE oriented gyres embedded with eddies: low SSHA (cyclonic) in winter and high SSHA (anticyclonic) in summer half year. The transition between these two basic patterns starts with a high/low SSHA tongue east of the Vietnam coast around 12° ~ 4°N in late winter/summer half year. This high/low SSHA grows gradually, first as a separate anti-cyclone/cyclone east off Vietnam and south of the Xisha Islands, and later develops into a big gyre while moving eastward to the deep basin.

More detailed patterns of the SCS circulation variability are extracted by the 3 × 4 SOM. Seasonal variation is found to dominate the SCS circulation variability. In winter (November—February), the SCS surface circulation is dominated by a basin-scale SW—NE oriented anti-cyclonic gyre embedded with eddies. In spring (March—April), a high SSHA tongue starts to grow east off Vietnam around 13°N, and develops as a big anticyclonic gyre while moving eastward to the deep water area; the general circulation is weak. In summer (May—July), the anticyclonic gyre fully expands to dominate the whole SCS with a SW—NE oriented axis embedded with eddies. In fall (August—October), a low SSHA tongue appears east off Vietnam around 12° ~ 14°N, and develops into a big cyclonic eddy between the two anticyclonic gyres in the northeastern and southwestern parts of the SCS, respectively; a dipole structure is formed southeast off Vietnam with a strong offshore jet. In either winter or summer, the alongshore current on the western boundary is intensified. The characteristic spatial patterns of the SCS surface circulation are consistent with the previous results (e.g., Li et al., 2003; Hwang and Chen, 2002).

Interannual variation of the SCS surface circulation is also revealed by the 3 × 4 SOM. Besides the strong 1997/1998 warm event in response to the strong Pacific El Nino in 1997, which is consistent with the previous results of other researchers (e.g., Wu and Chang, 2005; Xie et al., 2003; Wang et al., 2002), the overall SCS sea level is found to have a significant rise during 1999 ~ 2001, however, in summer 2004 the overall SCS sea level is lower and the basin-wide anticyclonic gyre (the SW—NE oriented high SSHA) becomes weaker than the other years. These new findings of interannual variation deserve further studies, especially to be evidenced from other data sets, such as SST.

For the first time, the SOM technology has been used to study upper layer circulation variability in the SCS. The representation of the multiyear SSHA

with the SOM spatial patterns and the BMU time series offers a new way to visualize the SCS circulation variability, which is otherwise not readily seen through conventional feature extraction methods, such as the temporal/spatial averaging and the EOF. This is the main advantage of the nonlinear neural network mapping that conserves the topology of the data. It is realized that the SOM results (patterns and the associated frequencies of occurrence) may be sensitive to the SOM parameter choices, however, the essential features are extracted with a proper selection of the parameters as demonstrated by Liu, Weisberg and Mooers (2006).

It should be noted that it is SSHA that is used in this analysis. The mean SSH and background circulation are not included. If the mean SSH is added back (e. g., Bao et al., 2005) or dynamic height from climatological hydrography (e. g., Li et al., 2003) or from a dynamical synthesis of the GRACE, AVISO, drifter and wind data are used instead (e. g., Liu et al., 2005), the circulation patterns may be different. Since an inaccurate mean SSH field may be misleading in the absolute SSH estimate, and a consensus on how to determine the mean SSH has not been reached, analysis of the absolute SSH field is not pursued here in this paper, however, it is worthwhile to be addressed in future studies.

Acknowledgements

Liu Yonggang would like to dedicate this paper to Professor Su Jilan for his 70th birthday celebration at the Second Institute of Oceanography, State Oceanic Administration of China. Liu Yonggang would like to thank Professor Su for his encouragements and invaluable guidance during the author's early career, and for his continued interest in the author's personal and professional growth. The SOM MATLAB Toolbox was provided by Alhoniemi E, Himberg J, Parhankangas J, and Vesanto J. The altimeter products were produced by SSALTO/DUACS as part of the Environment and Climate European Enact Project under contract EVK2-CT2001-00117 and distributed by AVISO, with support from CNES.

References

Bao L, Lu Y, Wang Y, et al. 2005. Seasonal variations of upper ocean circulation over the South China Sea from satellite altimetry data of many years. Chinese Journal of Geophysics, 48(3): 543 ~ 550

Cai S, Su J, Gan Z, et al. 2002. The numerical study of the South China Sea upper circulation characteristics and its dynamic mechanism in winter. Cont Shelf Res, 22:2247 ~ 2264

Cavazos T. 2000. Using self-organizing maps to investigate extreme climate events: an application to wintertime precipitation in the Balkans. J Climate, 13: 1718 ~ 1732

Chou D. 1982. Density circulation in the central water of South China Sea, Report of Comprehensive Survey in the Central South China Sea (1) in Chinese. Bejing: Science Press, 129 ~ 139

Chu P, Wang J, Qi Y. 2003. Determination of the South China Sea surface height variability using TOPEX/Poseidon data. Proc. SPIE Conf Remote Sensing Ocean and Sea Ice. Barcelona, Spain. 8-12 September 2003

Dale W L. 1956. Winds and drift currents in the South China Sea. Malay J Trop Geogr, 8: 1 ~ 31.

Ducet N, Le Traon P Y, Reverdin G. 2000. Global high resolution mapping of ocean circulation from TOPEX/Poseidon and ERS-1 and 2. J Geophys Res, 105: 19 477 ~ 19 498

Fang G, Fang W, Fang Y, et al. 1998. A survey of studies on the South China Sea upper ocean circulation. Acta Oceanogr Taiwan, 37: 1 ~ 16

Fang W, Guo Z, Huang Y. 1998. Observational study of the circulation in the southern South China Sea. Chinese Science Bulletin, 43 (11): 898 ~ 905

Fu L L, Cheney R E. 1995. Application of satellite altimetry to ocean circulation studies: 1987—1994. Rev Geophys, 33: 213 ~ 224

Guan B, Yuan Y. 2006. Overview of studies on some eddies in the China seas and their adjacent seas. Ⅰ: The South China Sea and the region east of Taiwan. Acta Oceanologi-

ca Sinica (in Chinese), 28: 1 ~ 16

Ho C R, Kuo N J, Zheng Q, et al. 2000. Dynamically active areas in the South China Sea detected from TOPEX/POSEIDON satellite altimeter data. Remote Sens. Environ, 71: 320 ~ 328

Ho C R, Zheng Q, Soong Y S, et al. 2 000. Seasonal variability of sea surface height in the South China Sea observed with TOPEX/POSEIDON altimeter data. J Geophys Res, 105: 13981 ~ 13990

Hong Y, Hsu K, Sorooshian S, et al. 2005. Self-organizing nonlinear output (SONO): a neural network suitable for cloud patch-based rainfall estimation at small scales. Water Resour Res, 41 W03008, doi:10. 1029/2004WR003142

Hsieh W W. 2001. Non-linear principal component analysis by neural networks. Tellus, 53: 599 ~ 615

Hsu K, Gupta H V, Gao X, et al. 2002. SOLO—An artificial neural network suitable for hydrologic modeling and analysis. Water Resources Research, 38: 1302 ~ 1318

Hu J, Kawamura H, Hong H, et al. 2000. A review on the currents in the South China Sea: seasonal circulation, South China Sea Warm Current and Kuroshio intrusion. J. Oceanogr, 56: 607 ~ 624

Hwang C, Chen S A. 2000. Circulations and eddies over the South China Sea derived from TOPEX/Poseidon altimetry. J Geophys Res, 105: 23943 ~ 23965

Jacobs G A, Barron C N, Rhodes R C. 2001. Mesoscale characteristics. J Geophys Res, 106: 19 581-19 595

Kaski S, Kangas J, Kohonen T. 1998. Bibliography of self-organizing map (SOM) papers: 1981 ~ 1997. Neural Comput Surv, 1: 102 ~ 350

Kohonen T. 1982. Self-organized information of topologically correct features maps. Bio Cyber, 43: 59 ~ 69

Kohonen T. 2001. Self-Organizing Maps. Springer Ser Inf Sci. v 30. 3rd ed. New York, Springer:501

Le Traon, P Y, Dibarboure G. 1999. Mesoscale mapping capabilities of multi-satellite altimeter missions. J. Atmos Oceanic Technol, 16: 1208 ~ 1223

Le Traon P Y, Dibarboure G, Ducet N. 2001. Use of a high-resolution model to analyze the mapping capabilities of multiple-altimeter missions. J Atmos Oceanic Technol, 18: 1277 ~ 1288

Le Traon P Y, Faugère Y, Hernandez F, et al. 2002. Can we merge GEOSAT follow-on with TOPEX/POSEIDON and ERS-2 for an improved description of the ocean circulation? J Atmos Oceanic Technol, 20: 889 ~ 895

Li L. 2002. Advance in observational studies of upper layer circulations of the South China Sea. J Oceanogr Taiwan Strait (in Chinese), 21(1): 114 ~ 125

Li L, Wu R, Guo X. 2000. Seasonal circulation in the South China Sea: a TOPEX/POSEIDON satellite altimetry study. Acta Oceanologica Sinica (in Chinese), 22(6): 13 ~ 26

Li L, Xu J, Jing C, et al. 2003. Annual variation of sea surface height, dynamic topography and circulation in the South China Sea. Science in China (D), 46: 127 ~ 138

Li R, Zeng Q, Ji Z, et al. 1992. Numerical simulation for a northeastward flowing current from area off the eastern Hainan Island to Tsugaru/Soya Strait. La Mer, 30: 229 ~ 238

Liu Q, Jia Y, Wang X, et al. 2001. On the annual cycle characteristics of the sea surface height in South China Sea. Advances Atmos Sci, 18: 613 ~ 621

Liu X, Su J. 1992. A reduced model of the circulation in the South China Sea. Oceanologia et Limnologia Sinica, 23 (2): 167 ~ 174

Liu Y, Weisberg R – H . 2007. Ocean currents and sea surface heights estimated across the West Florida Shelf. J Phys Oceanogr, 37(6):1697 ~ 1713

Liu Y, Weisberg R H. 2005. Patterns of ocean current variability on the West Florida Shelf using the self-organizing map. J Geophys Res, 110: C06003, doi: 10. 1029/2004JC002786

Liu Y, Weisberg R H, He R. 2006a. Sea surface temperature patterns on the West Florida Shelf using the growing hierarchical self-organizing maps. J Atmos Oceanic Technol, 23(2): 325 ~ 338

Liu Y, Weisberg R H, Mooers C N K. 2006b. Performance evaluation of the self-organizing map for feature extraction. J Geophys. Res, 111. C05018, doi. 10. 1029/2005jc003117

Liu Y, Weisberg R H, Shay L K. 2007. Current patterns on the West Florida Shelf from joint self-organizing map analyses of HF radar and ADCP data. J Atmos Oceanic Technol, 24(4):702 ~ 712

Liu W T, Xie X. 1999. Space-based observations of the seasonal changes of South Asian monsoons and oceanic response. Geophys Res Lett, 26: 1473 ~ 1476

Liu Q, Xie S P, Li L, et al. 2005. Ocean thermal advective effect on the annual range of sea surface temperature. Geo-

phys Res Lett, 32: L24604, doi:10.1029/2005GL024493

Liu Q, Yang H, Liu Z. 2001. Seasonal features of the Sverdrup circulation in the South China Sea. Progress in Natural Science, 11: 202 ~ 206

Liu Z, Yang H, Liu Q. 2001. Regional dynamics of seasonal variability in the South China Sea. J Phys Oceanogr, 31: 272 ~ 284

Liu Y, Yuan Y, Su J, et al. 2000. Circulation in the South China Sea in Summer of 1998. Chinese Science Bulletin, 45(18): 1 648 ~ 1 655

Mao Q, Shi P, Qi Y. 1999. Sea surface dynamic topography and geostrophic current over the South China Sea from Geosat altimeter observation. Acta Oceanologica Sinica + (in Chinese),21(1): 11 ~ 16

Metzger EJ, Hurlburt H E. 2001. The nondeterministic nature of Kuroshio penetration and eddy shedding in the South China Sea. J,Phys Oceanogr, 31(7): 1712 ~ 1732

Morimoto A, Yoshimoto K, Yanagi T. 2000. Characteristics of sea surface circulation and eddy field in the South China Sea revealed by satellite altimetric data. J Oceanogr, 56 (3): 331 ~ 344

Oja M, Kaski S, Kohonen T. 2002. Bibliography of self-organizing map (SOM) papers: 1998 ~ 2001 addendum. Neural Computing Surveys, 3: 1 ~ 156

Pohlmann T. 1987. A three dimensional circulation model of the South China Sea. In:Nihoul J C J,Jamar B M, eds. Three-Dimensional Models of Marine and Estuarine Dynamics,Elsevier, 245 ~ 268

Qiu D, Huang Y,Chen L, et al. 1985. Circulation structures in the studied waters. P. 204 ~ 230. In South China Sea Institute of Oceanology. Chinese Academy of Sciences,ed. Comprehensive Investigation and Studies of the South China Sea (2) (in Chinese). Beijing: Science Press

Qu T. 2000. Upper-layer circulation in the South China Sea. J Phys Oceanogr, 30: 1450 ~ 1460

Qu T, Du Y, Meyers G,et al. 2005. Connecting the tropical Pacific with Indian Ocean through South China Sea. Geophys Res Lett, 32: L24609, doi:10.1029/2005GL024698

Qu T, Kim Y Y, Yaremchuk M, et al. 2004. Can Luzon Strait transport play a role in conveying the impact of ENSO to the South China Sea? J Climate, 17: 3644 ~ 3657

Richardson A J, Risien C, Shillington FA. 2003. Using self-organizing maps to identify patterns in satellite imagery. Progr Oceanogr, 59: 223-239

Risien CM, Reason C J C , Shillington F A, et al. 2004. Variability in satellite winds over the Benguela upwelling system during 1999 ~ 2000. J Geophys Res, 109: C03010, doi:10.1029/2003JC001880

Shaw P T, Chao S Y. 1994. Surface circulation in the South China Sea. Deep-Sea Res, 41: 1663 ~ 1683

Shaw P T, Chao S Y, Fu L. 1999. Sea surface height variations in the South China Sea from satellite altimetry. Oceanol Acta, 22: 1 ~ 17

Soong Y S, Hu J H, Ho C R, et al. 1995. Cold core eddy detected in South China Sea. EOS, 76: 345 ~ 347

Su J, Xu J, Cai S, et al. 1999. Gyres and eddies in the South China Sea. In:Ding Y,Li C,eds. Onset and Evolution of the South China Sea Monsoon and Its Interaction with the Ocean(in Chinese). Bejing: China Meteorological Press, 272 ~ 279

SSALTO/DUACS User Handbook. 2004. (M)SLA and (M) ADT near-real time and delaued time products. CLS-DOS-NT-04. 103, France. Available online at http://www. jason. oceanobs. com/doucments/donnees/duacs/hanbook duacs. pdf

Takano K, Hahashima A, Namba T. 1998. A numerical simulation of the circulation in the South China Sea—Preliminary results. Acta Oceanogr. Taiwanica, 37: 165 ~ 186

Vesanto J, Himberg J, Alhoniemi E, et al. 1999. Self-organizing map in Matlab: the SOM Toolbox. Proceedings of the Matlab DSP Conference 1999. Espoo, Finland, November 1999, 35 ~ 40

Wang L, Koblinsky C J, Howden S. 2000. Mesoscale variability in the South China Sea from TOPEX/Poseidon altimetry data. Deep-Sea Res (Part I.), 47:681 ~ 708

Wang L, Koblinsky C, Howden S, et al. 1999. Interannual variability in the South China Sea from expendable bathythermograph data. J Geophys Res, 104(C10): 23509 ~ 23524

Wang G, Su J, Chu P. 2003. Mesoscale eddies in the South China Sea observed with altimeter data. Geophys Res Lett, 30: 2121, doi:10.1029/2003GL018532

Wang D, Xie Q, Du Y,et al. 2002. The 1997 ~ 1998 warm event in the South China Sea. Chin Sci Bull, 47: 1221 ~ 1227

Wang H, Yuan Y, Guan W, et al. 2004. Circulation in the South China Sea during summer 2000 as obtained from observations and a generalized topography-following ocean

model. J Geophys Res, 109, C07007, doi: 10. 1029/2003JC002134

Wyrtki K. 1961. Physical oceanography of Southeast Asian waters. Naga Rep, V2. San Diego: Univ of Calif, 195

Wu C R, Chang C W J. 2005. Interannual variability of the South China Sea in a data assimilation model. Geophys Res Lett, 32: L17611, doi:10.1029/2005GL023798

Wu C R, Shaw P T, Chao S Y. 1998. Seasonal and interannual variations in the velocity field of the South China Sea. J Oceanogr, 54: 361 ~ 372

Wu C R, Tang T Y, Lin S F. 2005. Intra-seasonal variation in the velocity field of the northeastern South China Sea. Cont Shelf Res, 25(17): 2 075 ~ 2 083

Xie S P, Xie Q, Wang D. 2003. Summer upwelling in the South China Sea and its role in regional climate variations. J Geophys Res, 108 (C8): 3261, doi: 10. 1029/2003JC001867

Xu J, Li L, Guo X, et al. 2001. Multi-eddy (in Chinese) China Sea circulation around onset of summer monsoon in 1998. J Tropic Oceangr (in Chinese), 20(1): 44 ~ 51

Xu X, Zhang Q, Chen H. 1982. The general descriptions of the horizontal circulation in the South China Sea. Proc Symp of the Chinese Society of Marine Hydrology and Meteorology (in Chinese), 119 ~ 127

Yuan Y, Bu X, Liao G, et al. 2004. Diagnostic calculation of the upper-layer circulation in the South China Sea during the winter of 1998. Acta Oceanologica Sinica, 23(2): 187 ~ 199

Yuan Y, Liu Y, Liao G, et al. 2005. Calculation of circulation in the South China Sea during summer of 2000 by the modified inverse method. Acta Oceanologica Sinica, 24(1): 14 ~ 30

Zeng Q, Li R, Ji Z, 1989. Calculations of the monthly mean circulation in the South China Sea. Scientia Atmospherica Sinica (in Chinese), 13: 127 ~ 168

Zhou F, Shen J, Berestov A, et al. 1995. Seasonal features of large-scale geostrophic circulations in the South China Sea. J Tropic Oceanogr (in Chinese), 14(4): 9 ~ 14